Anand Karpatne
Department of Aerospace
and Engineering Mechanics,
University of Texas,
Austin, TX 78712
e-mail: anand.karpatne@utexas.edu

Jayant Sirohi
Assistant Professor
Department of Aerospace
and Engineering Mechanics,
University of Texas,
Austin, TX 78712
e-mail: jayant.sirohi@utexas.edu

Swathi Mula
Department of Aerospace
and Engineering Mechanics,
University of Texas,
Austin, TX 78712
e-mail: swathimula.ae@utexas.edu

Charles Tinney
Assistant Professor
Department of Aerospace
and Engineering Mechanics,
University of Texas,
Austin, TX 78712
e-mail: cetinney@utexas.edu

Vortex Ring Model of Tip Vortex Aperiodicity in a Hovering Helicopter Rotor

The wandering motion of tip vortices trailed from a hovering helicopter rotor is described. This aperiodicity is known to cause errors in the determination of vortex properties that are crucial inputs for refined aerodynamic analyses of helicopter rotors. Measurements of blade tip vortices up to 260 deg vortex age using stereo particle-image velocimetry (PIV) indicate that this aperiodicity is anisotropic. We describe an analytical model that captures this anisotropic behavior. The analysis approximates the helical wake as a series of vortex rings that are allowed to interact with each other. The vorticity in the rings is a function of the blade loading. Vortex core growth is modeled by accounting for vortex filament strain and by using an empirical model for viscous diffusion. The sensitivity of the analysis to the choice of initial vortex core radius, viscosity parameter, time step, and number of rings shed is explored. Analytical predictions of the orientation of anisotropy correlated with experimental measurements within 10%. The analysis can be used as a computationally inexpensive method to generate probability distribution functions for vortex core positions that can then be used to correct for aperiodicity in measurements. [DOI: 10.1115/1.4026859]

1 Background and Motivation

1.1 Introduction. The aerodynamic environment of a helicopter rotor is very complicated due to the presence of a vortex-dominated wake in close proximity to the rotor disk that significantly affects the flow field around the rotor. The wake of each rotor blade is composed of two parts—an inboard vortex sheet and a concentrated tip vortex. For a rotor in hover, the wake is axisymmetric and is dominated by the helical tip vortex trailed by each rotor blade [1]. Several characteristics of tip vortices, such as vortex core radius and swirl velocity, can be extracted from rotor wake velocity measurements. These characteristics are very important for refined modeling of helicopter rotor wakes and, consequently, in the design of advanced rotors with improved efficiency.

The measurement of tip vortex velocity profiles is complicated by the phenomenon of vortex wandering. This is defined as a small random motion of the vortex core perpendicular to the axis of the vortex filament. It is observed in both fixed-wing as well as rotary-wing tip vortices. In the latter case, the vortex wandering motion is also called aperiodicity because it results in aperiodic motion of the tip vortex core at a given azimuthal position or vortex age (azimuthal angle since the tip vortex was trailed). Typically, the standard deviation of the axial and radial positions of the tip vortex core increases with wake age and are on the order of 5%–10% of the blade chord.

Several researchers have observed the phenomenon of rotor tip vortex aperiodicity and have proposed methods to correct the measurements for this effect. Early research efforts used single-point measurement techniques such as hot-wire anemometry (HWA) or laser Doppler velocimetry (LDV) to measure the flow field of vortices from fixed-wing and rotary-wing tips (see the work of Devenport et al. [2] and Leishman [3]). The aperiodicity was determined to be isotropic, i.e., the standard deviation in measured position of the tip vortex core was identical in all directions. Therefore, an isotropic, Gaussian probability distribution function was used to determine the true velocity field in an iterative manner by comparing the calculated velocity field to the measurements.

Developments in whole-field optical measurement techniques, such as stereoscopic particle image velocimetry (stereo-PIV), have enabled instantaneous measurements of the velocity field over a large region of interest. Bhagwat and Ramasamy [4] used PIV measurements of tip vortex velocity fields to illustrate the errors introduced by aperiodicity. They discussed methods of correcting aperiodicity and show that analytical methods used to extract vortex properties that are based on the global velocity field are less sensitive to aperiodicity corrections than methods based on local data. The whole-field capability of PIV has yielded more insight into the phenomenon of aperiodicity. Richard et al. [5] obtained two- and three-component PIV measurements on a reduced scale rotor and performed a parametric study to determine the optimum interrogation window size and overlap parameter. To obtain a reliable analysis of the vortex core parameters, the data obtained from three-component PIV measurements need to be corrected for aperiodicity, turbulence, vortex wander, and other effects. Some of these corrective methods are described by Van der Wall and Richard [6]. Kindler et al. [7] measured the wake of a full-scale, four-bladed hingeless rotor using stereo-PIV and found that the aperiodicity was anisotropic, i.e., the standard deviation of the center of the tip vortex was larger along the axial direction than along the radial direction of the rotor wake. However, their measurements were confined to wake ages between

Contributed by the Fluids Engineering Division of ASME for publication in the Journal of Fluids Engineering. Manuscript received June 20, 2013; final manuscript received February 5, 2014; published online May 6, 2014. Assoc. Editor: Zhongquan Charlie Zheng.

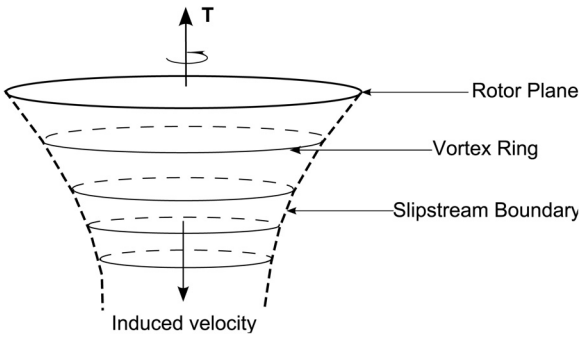

Fig. 1 Oblique view of vortex rings convecting downstream

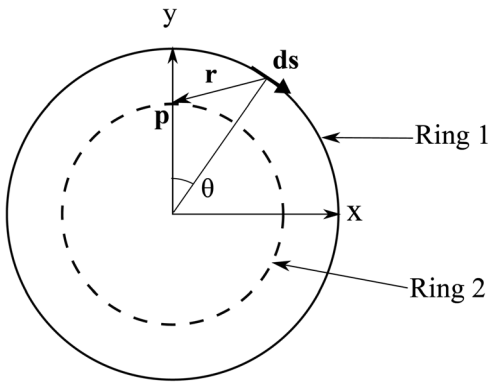

Fig. 2 Top view of vortex ring geometry showing two vortex rings. Element ds on ring 1 induces a velocity on ring 2.

0 deg and 30 deg. Stereo-PIV measurements performed by Mula et al. [8] on a 1 m diameter, four-bladed rotor in hover confirmed the anisotropic nature of tip vortex aperiodicity for vortex ages up to 260 deg. They also observed that the 95% confidence region for the tip vortex center was elliptical in shape with its major axis aligned perpendicular to the slipstream boundary.

A number of vortex-based techniques have been developed to model the wake of a rotor. The most popular technique is the free wake method [9], which involves discretizing the rotor wake into small vortex filaments and then calculating the velocities induced by the filaments on each other using either a relaxation-based approach or a time-marching approach. The latter, being time accurate, can also be used to model transient flight conditions [10,11]. The effects of vortex filament strain and viscous diffusion must be included for these models to accurately predict the core radius growth [12–14].

For accurate predictions of the aerodynamic performance of a rotor using refined vortex-based analyses, it is essential to properly correct for errors introduced by aperiodicity and minimize uncertainty in the calculation of vortex properties from flow field measurements. In this paper, we describe an analytical model based on approximating the helical wake of a hovering rotor as a series of vortex rings. The rings are allowed to interact due to their induced velocity distribution and the resulting motion is calculated using time marching. This approach can be used to calculate an anisotropic probability distribution function for the vortex core positions, with a minimum of computational effort.

In this paper, we describe the development of a vortex ring emitter model (VREM) and use it to investigate the phenomenon of tip vortex aperiodicity in a hovering rotor. The VREM approximates the axisymmetric wake of a hovering rotor as a series of vortex rings that are allowed to freely convect and strain under their induced velocity field. Brand et al. [15] used this approach to investigate the vortex ring state and obtained a good physical insight into the behavior of the rotor wake at low computational cost. We explore the sensitivity of the VREM to a number of model parameters such as initial tip vortex core radius, vorticity parameter, time step, and number of rings emitted. Finally, VREM predictions of the extent of vortex aperiodicity are correlated with experimental measurements. The VREM can be used to generate an anisotropic probability function for the tip vortex position at a low computational cost.

2 Analytical Approach

The methodology behind the VREM is based on the underlying assumption of axisymmetric flow during hover. Vortex rings convect downstream under the influence of their induced velocities. Their core growth is modeled to include the effects of both filament strain and viscous diffusion. A predictor-corrector time-marching scheme is then used to convect the rings in time. A description of this methodology is provided in the following subsections.

2.1 Vortex Ring Representation. The wake of a hovering rotor is approximated by a series of toroidal vortex rings that are emitted by each rotor blade once per revolution (Fig. 1). This is a satisfactory approximation of the wake for rotors operating at low to moderate thrust levels, where the induced velocity and wake helix angle are small. The entire vorticity over the blade span is trailed at the rotor tip and the effects of the inboard vortex sheet are ignored. This assumption is made because the gradient in bound circulation over the rotor blade span is maximum near the tip of the rotor blade. Therefore, the tip vortex plays a dominant role in the development of the rotor wake. Other models reported in the literature have also simplified the rotor wake in this manner by considering only the effects of the tip vortices (see McCroskey [16]). In the present analysis, the velocity field induced by the vortex rings is calculated using the Biot–Savart law. The vortex rings are allowed to convect freely and distort due to this induced velocity field. The cross section of each vortex ring is assumed to remain circular at all times, although the radius of the core is allowed to change based on the effects of stretching and viscous diffusion.

The top view of a pair of vortex rings is shown in Fig. 2. Ring 1 has a radius R_1 and a circulation strength Γ. The velocity $\mathbf{dv}$ induced on ring 2 by the element $\mathbf{ds}$ on ring 1 is calculated as

$$\mathbf{dv_i} = \frac{\Gamma}{4\pi}\frac{\mathbf{ds}\times\mathbf{r}}{\left(|\mathbf{r}|^2 + r_{\text{core}}^2\right)^{\frac{3}{2}}} \tag{1}$$

where r_{core} is the core radius of vortex ring 1 and $\mathbf{r}$ is the position vector of the point $\mathbf{p}$ from the element.

The elemental induced velocity $\mathbf{dv_i}$ is integrated over the circumference of the vortex ring 1, through an angle θ ranging from 0 to 2π radians. In this way, the total radial (V_{ix}) and axial velocities (V_{iz}) induced by the ring at the point $\mathbf{p}$ on ring 2 are obtained as

$$V_{ix} = \frac{\Gamma}{4\pi}\int_0^{2\pi}\frac{(R_1 z_p\cos\theta)d\theta}{(L^2 - 2R_1 x_p\cos\theta)^{\frac{3}{2}}} \tag{2}$$

$$V_{iz} = \frac{\Gamma}{4\pi}\int_0^{2\pi}\frac{(R_1^2 - R_1 x_p\cos\theta)d\theta}{(L^2 - 2R_1 x_p\cos\theta)^{\frac{3}{2}}} \tag{3}$$

where the parameter $L^2 = x_p^2 + z_p^2 + R_1^2 + r_{\text{core}}^2$. These elliptic equations are solved using a trapezoidal integration scheme with 1000 integration points along the circumference of the vortex ring. In this way, the radial and axial velocities induced by a ring on any other ring, as well as upon itself, are obtained.

2.2 Treatment of Core Radius. The core radius of the vortex ring plays an important role in evaluating induced velocities (Eqs. (2) and (3)), especially when calculating self-induced

velocities. Therefore, it is necessary to model the development of the core radius over time. Two factors that have a profound effect on vortex core growth are: vortex filament strain and viscous diffusion. These were studied independently and a combined core growth model was developed.

2.2.1 Vortex Filament Strain. The radius of any emitted vortex ring changes with time due to the various radial velocities imparted to it. The ratio of the change in length of a vortex filament to the original length is known as vortex filament strain. Because the vortex rings are assumed to convect in an inviscid fluid, the total circulation of a vortex ring is conserved throughout its existence. Moreover, the maximum magnitude of the vortex core swirl velocity has been measured to be on the order of 10% V_{tip} [17]. This suggests that the flow can be treated as incompressible, and hence, the conservation of circulation leads to the conservation of volume of the toroidal ring. Assuming that the radius of the vortex ring at the time of emission is R_0 (same as rotor radius R), and the initial core radius is $r_{\text{core},0}$, the volume of the ring is $V = 2\pi R_0 \pi r_{\text{core},0}^2$. To conserve the volume of the ring we can calculate the new core radius of the ring at a vortex age ζ as follows:

$$r_{\text{core},\zeta,s} = r_{\text{core},0}\sqrt{\frac{R_0}{R_\zeta}} \tag{4}$$

2.2.2 Viscous Diffusion. Viscous diffusion leads to an expansion of the vortex core and a decrease in the maximum magnitude of vortex swirl velocity with time. Consequently, the volume of the toroidal vortex is no longer conserved. However, total circulation and angular momentum are conserved. If the vortex wake structure is considered to be highly turbulent, a simple laminar viscosity model (for example, Lamb Oseen's) would prove insufficient. Therefore, following the approach of Bhagwat et al. [13], the core radius growth is approximated by

$$r_{\text{core},\delta} = \sqrt{4\alpha_L \delta \nu t} \tag{5}$$

where the Squire's model [18] is used to represent the viscous effects. The viscosity parameter δ is representative of the turbulent viscosity in the medium and is empirically obtained, $\alpha_L = 1.25643$ is Lamb's constant, ν is the coefficient of viscosity, and t is the time elapsed since the formation of the tip vortex. Note that δ depends on the vortex Reynolds number, which was obtained from measurements on our experimental setup. By establishing an initial core radius, $r_{\text{core},0}$ at 0 deg vortex age and replacing time by ζ/Ω, the vortex core radius is

$$r_{\text{core},\zeta,\nu} = \sqrt{r_{\text{core},0}^2 + 4\alpha_L \delta \nu \frac{\zeta}{\Omega}} \tag{6}$$

2.2.3 Combined Core Growth. The effects of both filament strain and viscous diffusion are combined to obtain a model for the vortex core radius at any vortex age. Changes in radius Δr_s and Δr_{diff} due to strain and diffusion, respectively, are calculated independently (Eqs. (7) and (8)) and their effects combined using Eq. (9) to determine the final core radius. Here, the effect of viscosity in the near rotor wake acts to increase the growth of the core radius in addition to the effect of filament strain.

$$\Delta r_s = r_{\text{core},0}\sqrt{\frac{R_0}{R_\zeta}} - r_{\text{core},0} \tag{7}$$

$$\Delta r_{\text{diff}} = \sqrt{r_{\text{core},0}^2 + 4\alpha_L \delta \nu \frac{\zeta}{\Omega}} - r_{\text{core},0} \tag{8}$$

$$r_{\text{core}} = r_{\text{core},0} + \Delta r_s + \Delta r_{\text{diff}} \tag{9}$$

The growth of the vortex core can be modeled using a number of different approaches; this model was chosen for the present study due to its ease of implementation.

2.3 Time-Stepping Solution Scheme. The total velocity field induced by all the rings must be calculated at each time step. It is known that certain time integration schemes generate numerical instabilities that can result in aperiodicity of the calculated tip vortex positions [10,19]. For example, it was observed that an explicit time-advancing scheme was not stable for predicting the motion of vortex rings. Therefore, a trapezoidal predictor-corrector scheme was chosen for time stepping as shown in the following equations:

$$r_i^* = r_i^n + \Delta t V_{ix}\left(r_i^n, z_i^n\right) \tag{10}$$

$$z_i^* = z_i^n + \Delta t V_{iz}\left(r_i^n, z_i^n\right) \tag{11}$$

$$r_i^{n+1} = r_i^n + \frac{\Delta t}{2}\left[V_{ix}\left(r_i^*, z_i^*\right) + V_{ix}\left(r_i^n, z_i^n\right)\right] \tag{12}$$

$$z_i^{n+1} = z_i^n + \frac{\Delta t}{2}\left[V_{iz}\left(r_i^*, z_i^*\right) + V_{iz}\left(r_i^n, z_i^n\right)\right] \tag{13}$$

Equations (10) and (11) are used to predict an intermediate solution for radial and axial positions of the ring $\left(r_i^*, z_i^*\right)$ using an Euler scheme. Thereafter, velocities $\left(V_{ix}\left(r_i^*, z_i^*\right), V_{iz}\left(r_i^*, z_i^*\right)\right)$ are calculated at this new position (r_i^*, z_i^*). An average of the intermediate and the new velocities is used to find the position of the ring (Eqs. (12) and (13)).

The rotor blade is discretized into several spanwise segments (N) and the axial velocity induced by the rings is evaluated at each segment. This affects the local blade angle of attack:

$$\alpha_i = \theta_0 - \tan^{-1}\frac{V_{iz}}{\Omega r} \tag{14}$$

Correspondingly, the local lift coefficient $C_l(i)$ is calculated for each α_i from a lookup table for airfoil data. The total thrust T produced by the rotor is

$$T = \sum_{i=1}^{N} N_b \frac{1}{2}\rho\left(V_{iz}^2 + (\Omega r(i))^2\right) C_l(i) c(i) \frac{R}{N} \tag{15}$$

where i is the blade segment number, V_{iz} is the locally induced axial velocity, and Ωr is the local radial velocity. This time-varying lift is responsible for an adjustment in the vortex circulation strength for the next time step. The Kutta–Joukowski theorem is used for every spanwise element on the rotor blade to evaluate the bound circulation strength. The total thrust generated by one rotor blade in terms of an equivalent uniform bound circulation is given as

$$T = \Gamma \rho \int_0^R \Omega r dr \tag{16}$$

By summing the thrust over all the blades and assuming that the entire bound circulation is trailed at the tip, the circulation strength of the emitted vortex ring is given as

$$\Gamma = \frac{2T}{\rho N_b R V_{\text{tip}}} \tag{17}$$

where Γ is the circulation of the emitted tip vortex ring. This iterative process of calculating Γ is continued at each time step.

The VREM was written in FORTRAN 2003 and was compiled using an Intel IFORT compiler with second order optimization, on an Intel(R) Pentium (D) central processing unit, 64 bit operating system, with 3.60 GHz processing speed and 2 GB RAM. The

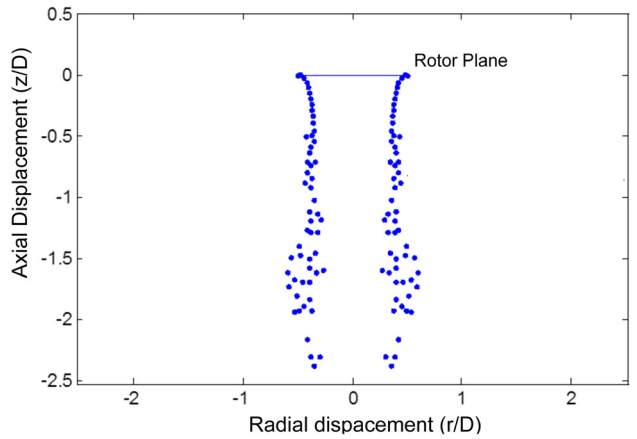

Fig. 3 Analytical predictions of tip vortex core positions normalized by rotor diameter D at a blade loading $C_t/\sigma = 0.042$. Model parameters: number of vortex rings emitted = 120, rotational speed = 1520 rpm, $\delta = 4$, initial core radius = 0.0081 m (0.14c).

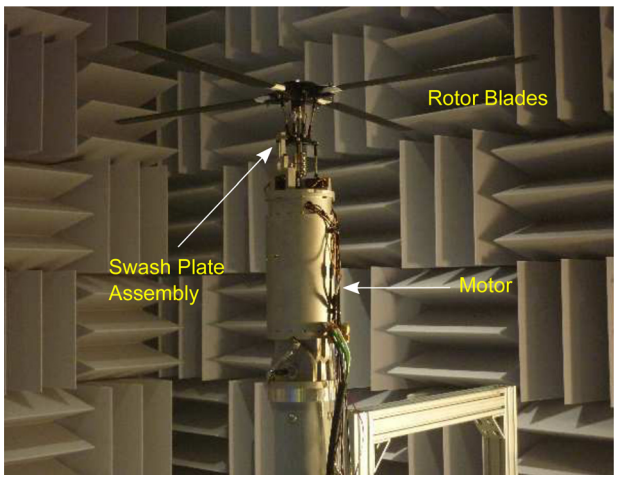

Fig. 4 Rotor test stand with 1 m diameter, four-bladed, articulated rotor [8]

processing time taken to run the simulation was proportional to $\sim N^3$, where N is the total number of rings emitted in the system. For 1000 rings emitted, the processing time was 830 s (~14 min). A snapshot of the slipstream after the emission of 120 rings ($C_t/\sigma = 0.042$) is shown in Fig. 3, which shows a well-defined slipstream boundary near the rotor. This was calculated using experimentally measured values of $r_{core} = 0.14c$ and a viscosity parameter of $\delta = 4$. Here, we see that as the vortex rings convect downstream, their interactions become more prominent and the slipstream boundary begins to diffuse.

3 Experimental Setup

To validate the VREM, experiments were conducted on a reduced-scale, four-bladed, articulated rotor in hover. The goal of these experiments was to capture the average positions of the tip vortices as well as their dynamic evolution for various vortex ages. An illustration of this rotor test stand is shown in Fig. 4. The rotor was driven by a direct drive, dc brushless rotor with a maximum rated power of 9 kW. Custom-fabricated optical encoders were used to monitor rotor speed as well as phase align the position of the blades with flow-sensing instruments. Relevant parameters and test conditions of the rotor are shown in Table 1.

Table 1 Parameters and test conditions of the rotor system

Number of blades	4
Diameter (m)	1.01
Chord (m)	0.0585
Twist (deg)	0
Blade airfoil	NACA0012
Blade tip shape	Square
Collective (deg)	7.2
Rotational speed (rpm)	1520
Tip speed (m/s)	80.33
Tip Reynolds number	248,000
Tip Mach number	0.23
C_t/σ	0.042
$\mathrm{Re}_\nu = \Gamma/\nu$	20,000

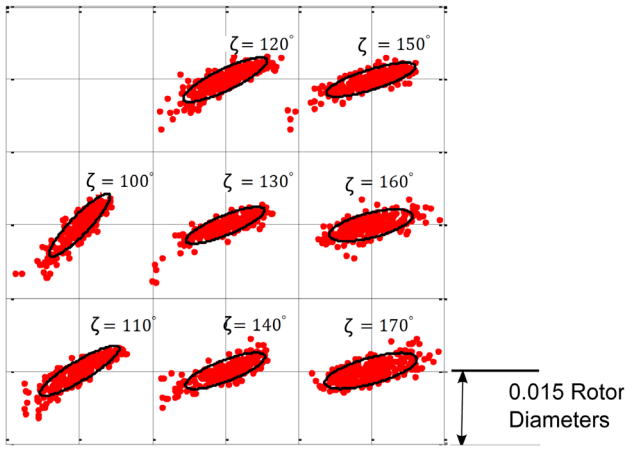

Fig. 5 Schematic illustrating the 95% confidence intervals for tip vortex core positions at various vortex ages ζ (ranging from 100 deg to 170 deg). Each dot indicates instantaneous tip vortex core position at a particular vortex age.

Measurements of the flow along a section through the rotor slipstream were performed using a stereo-PIV system. Two 2 M pixel CCD cameras with 14 bit resolution and 7 Hz (double frame mode) sampling frequency were used. Seeding was provided by a Laskin nozzle olive oil seeder with particles ranging between 0.1 and 1 μm in diameter. Tests were conducted by phase aligning the first PIV laser pulse with the quarter-chord location of the blades. A total of 36 phase-locked positions were studied ($\Delta\zeta = 10$ deg), each comprising 250 statistically independent image pairs. or a sample wake age of 30 deg, the maximum out-of-plane velocity was on the order of 10% V_{tip}. Coupled with an interframe timing rate of 110 μs and a 2 mm laser sheet thickness, this resulted in an out-of-plane particle displacement of less than 50% of the laser sheet thickness. Likewise, the accuracy of the measurements is to within 1 deg in azimuth, based on the rotation speed of the rotor and the interframe timing rate. Raw images were converted into vector maps using commercial software Davis v7.2 from LaVision GmbH using a final interrogation window of 16×16 pixels with 50% overlap. The calibration was performed using a pinhole-based model followed by the LaVision self-calibration tool set. Additional details regarding the experiment are described by Mula et al. [8].

To determine the instantaneous vortex center, a derivative-based technique termed the Q criterion/center of mass (Q/CoM) method [8] was applied to each PIV vector map. In doing so, a distinct aperiodicity in the position of the tip vortex cores was revealed, as shown in Fig. 5. A region of 95% confidence for the center of the vortex core was calculated for several vortex ages to estimate the direction and magnitude of the aperiodicity. From Fig. 5, it can be seen that the 95% confidence region has a

Table 2 Baseline parameters used in the VREM

Parameter	Value
r_{core} (initial)	$0.14c$ (0.0081 m)
Viscosity parameter (δ)	4
Time step (Δt)	0.0099 s
Number of rings emitted	1000

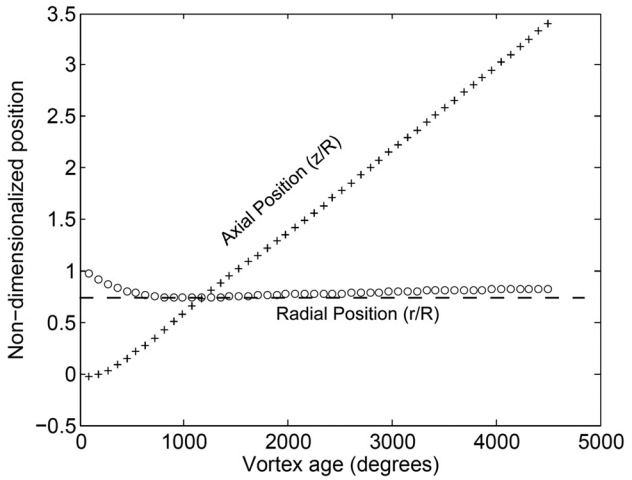

Fig. 6 Baseline case: mean slipstream boundary (axial (*z/R*) and radial (*r/R*)) as a function of vortex age, averaged over 1000 emitted rings

preferred orientation with its major axis aligned approximately perpendicular to the slipstream boundary.

A value of $r_{core} = 0.14c$ was measured at a vortex age of 10 deg. This was used as the initial core radius for the VREM. The viscosity parameter, $\delta = 4$, was estimated from the vortex Reynolds number of this experiment as described in Sec. 2.2.2.

4 Results and Discussion

The goal of the VREM is to predict the statistics of tip vortices emitted by a rotor in hover. The sensitivity of the VREM to input parameters was explored to determine optimum values for these parameters and accurate determination of the vortex aperiodicity. The results of the analysis were then compared with experimental measurements.

4.1 Sensitivity Studies. The sensitivity of the VREM to the following input parameters was studied:

(i) initial tip vortex core radius r_{core}
(ii) viscosity parameter δ
(iii) time step Δt
(iv) number of vortex rings emitted

The sensitivity study was performed by varying these parameters from their baseline values (shown in Table 2) and observing their effects on mean slipstream boundary as well as total rotor thrust.

4.1.1 Mean Slipstream Boundary. The mean axial and radial positions of the tip vortices as a function of vortex age are shown in Fig. 6 for the baseline case, which means that this represents an average over 1000 emitted rings. It can be seen that the shape of the slipstream boundary is as expected (see Ref. [1]) and the wake contracts for a vortex age up to ~1500 deg.

4.1.2 Total Rotor Thrust. The thrust produced by the rotor for the baseline case as a function of vortex age is plotted in Fig. 7.

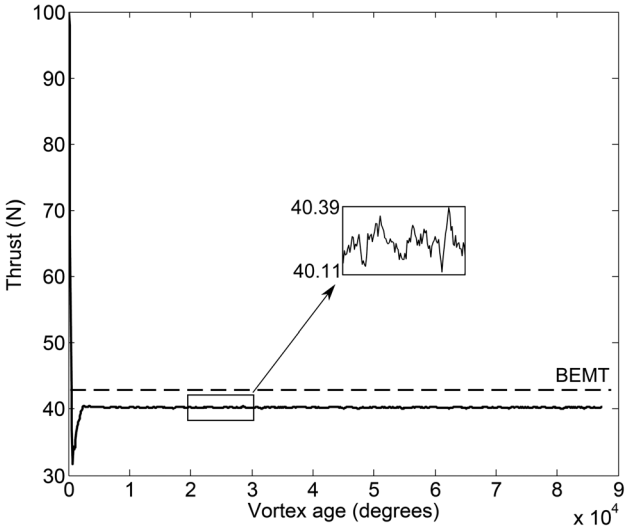

Fig. 7 Baseline case: thrust produced by the rotor as a function of vortex age, as predicted by the VREM. Thrust was computed until 1000 rings were emitted from the rotor blade. The thrust estimated from BEMT is shown as a dotted line.

This illustration represents a rotor instantaneously started from rest. An initial guess for thrust was chosen as 100 N. After 60 rings were emitted, the vortex circulation strength and the thrust generated by the rotor stabilized. However, minor fluctuations in the instantaneous thrust on the order of <0.5 % of the mean were still present in the system (see subset window). These fluctuations may be attributed to the wandering of the tip vortices, especially in the near wake of the rotor. Also, shown in this figure is the steady state rotor thrust predicted from blade element momentum theory (BEMT). It is seen that BEMT overpredicts the thrust by about 5% when compared to the VREM case.

4.1.3 Spanwise Loading. The spanwise loading (elemental coefficient of thrust dC_t) calculated by the VREM and the BEMT are shown in Fig. 8. Because the VREM ignores the inboard vorticity and assumes a concentrated tip vortex ring, it predicts a negative angle of attack over a large inboard section of the rotor blade. Although the total thrust predicted by the VREM is in close agreement with the BEMT prediction, underpredicting it by 5%, the VREM is limited in its ability to calculate spanwise loading due to its simplifying assumptions.

4.1.4 Initial Tip Vortex Core Radius. The baseline value of initial tip vortex core radius was measured from our experiments to be $r_{core} = r^* = 0.14c$. The initial vortex core radius was varied from the baseline value of $r_0 = r^*$ to $r_0 = 2.5r^*$ and its effect on the mean slipstream boundary as well as total rotor thrust was obtained. From Fig. 9, it can be concluded that the shape of the slipstream boundary is insensitive to initial core radius. The percentage difference in thrust from the baseline case is shown in Fig. 10 as a function of vortex age. It is seen that, initially (between vortex ages 0 deg to 2000 deg), an increase in initial core radius results in fluctuations in thrust difference from the baseline value. This trend is expected because immediately after the rotor starts emitting rings, the vortex rings are located very close to the rotor plane. Therefore, a change in the initial core radius causes large fluctuations in the velocities induced on the rotor blades. Moreover, the circulation strength of these vortex rings is also high as our initial guess for rotor thrust was much higher than the steady state value. Therefore, the effect of these vortex rings in the vicinity of the blade is pronounced and large fluctuations in the difference of predicted thrust from baseline value is obtained. However, as more rings are shed, these vortex rings (with large circulation strengths) are convected away from the rotor and their

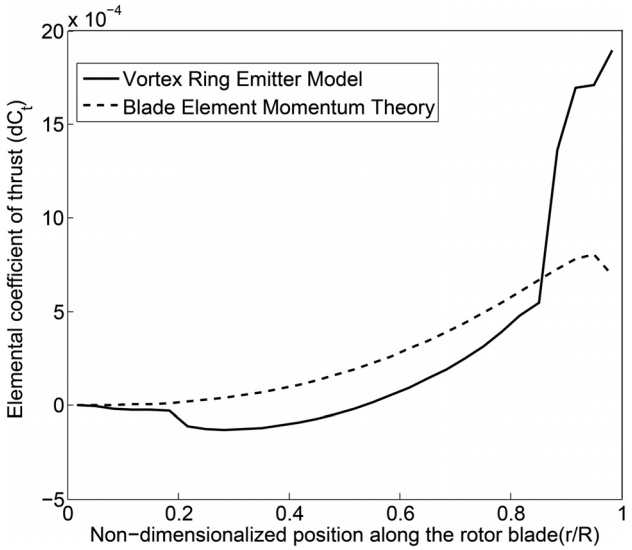

Fig. 8 Baseline case: spanwise loading predicted by the VREM and BEMT after 1000 vortex rings are emitted

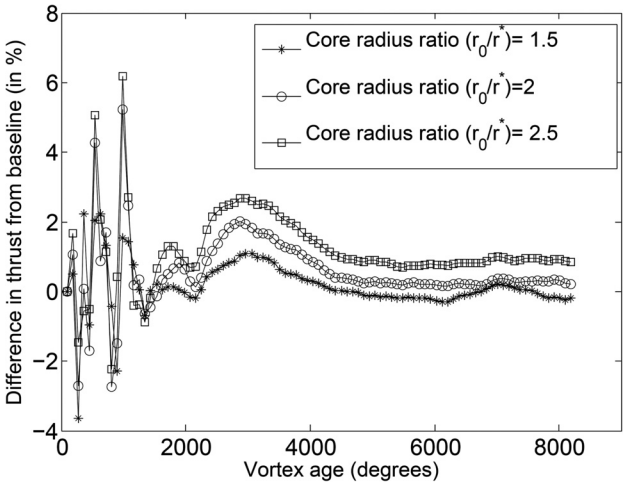

Fig. 10 Difference in the predicted thrust from baseline for various values of initial tip vortex core radius. The baseline thrust is calculated for $r_{core} = 0.14c$.

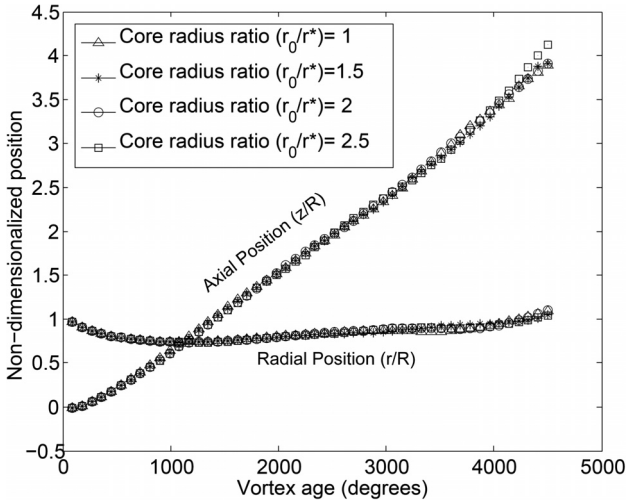

Fig. 9 Effect of initial tip vortex core radius on mean slipstream boundary. The baseline value of $r^* = 0.14c$ is based on experimental measurements.

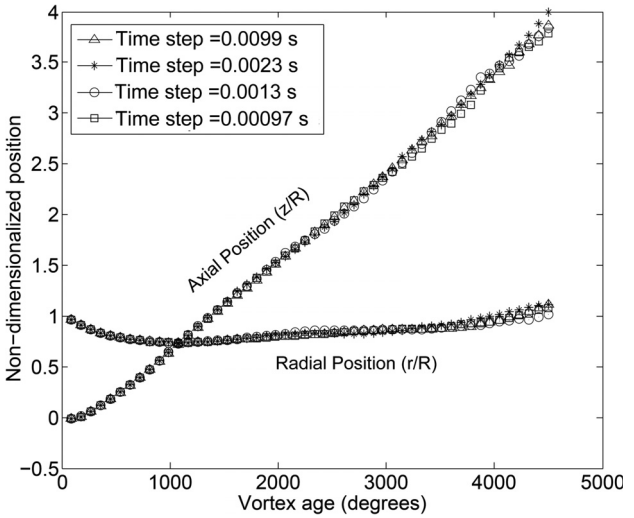

Fig. 11 Variation of the mean slipstream boundary for various values of time step

effects on the rotor blade are reduced and steady state thrust is obtained. If the initial core radius of the vortex rings was increased, their effects on each other and on the rotor plane would diminish much quicker than the baseline case, and faster convergence to steady state thrust could be obtained. In Fig. 10, it is seen that between vortex ages 2000 deg to 3000 deg, an increase in initial core radius causes the predicted thrust to increase more rapidly and reach steady state compared to the baseline. Beyond this point, the baseline thrust continues to increase while the predicted thrust corresponding to larger initial core radii cases has already reached steady state. This is observed in the figure as the difference in the predicted thrust from baseline shows a decrease between vortex ages 3000 deg and 4000 deg. Once the baseline case also attains a steady thrust value (as more rings are shed), a constant difference in the predicted thrust from baseline is seen (vortex ages beyond 4000 deg). Finally, it can be concluded that an increase in the initial core radius results in a slight increase in the steady state rotor thrust. As the core radius is increased, the velocity induced by the vortex rings on the rotor blade reduces and the local angle of attack on the blade is increased. This results in an increased total rotor thrust. However, this effect is small as the steady state thrust varies by less than 2%. Overall, it was observed that the effect of initial core radius was negligible on the VREM results. This is because the core radius plays a dominant role in the calculation of induced velocities only when the vortex rings are very close to each other (Eq. (1)). However, at steady state, the distance between vortex rings is several times larger than their core radii, especially in the near wake of the rotor. Therefore, the effect of vortex core size is not prominent in the VREM results.

4.1.5 Viscosity Parameter. An increase in the value of viscosity parameter δ results in an increase in the core radius growth rate. However, a change in the core radius did not have any significant effect on the mean slipstream shape or total rotor thrust. Therefore, the VREM predictions are expected to be insensitive to the choice of viscosity parameter.

4.1.6 Time Step. Because a vortex ring is emitted by each blade once per revolution, the time step Δt is the blade passage time. This depends on the rotational speed of the rotor as well as the total number of blades, so that $\Delta t = \Delta\zeta/\Omega$, where $\Delta\zeta = 2\pi/N_b$. The rotational speed was varied to obtain different time steps.

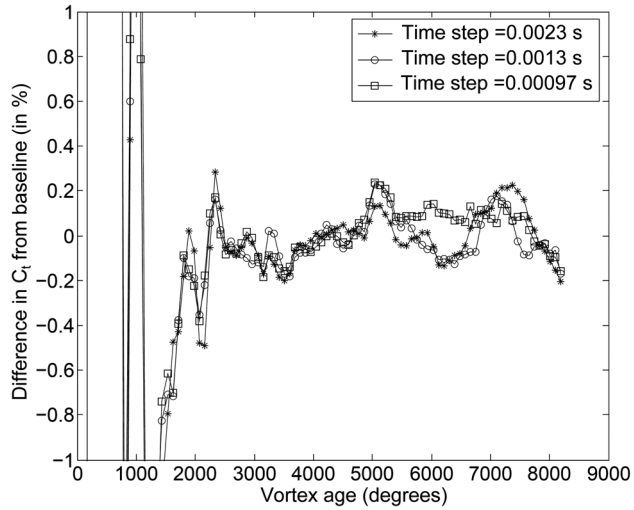

Fig. 12 Difference in the predicted thrust coefficient from baseline ($\Delta t = 0.0099$ s) for various values of time step

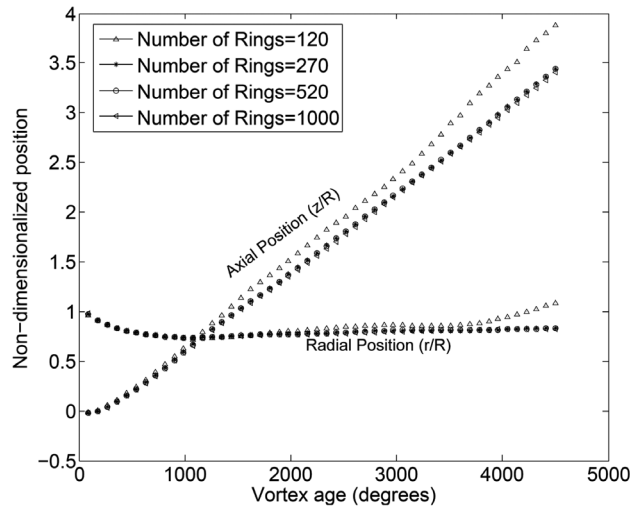

Fig. 13 Effect of the number of emitted rings on the slipstream boundary

Note that for a given blade angle of attack, changing the rotational speed changes the thrust of the rotor. However, the normalized aerodynamics of the rotor remains the same, as the total blade loading (C_t/σ) remains constant. The rotational speed was varied from 1520 rpm ($\Delta t = 0.0099$ s) to 15,520 rpm ($\Delta t = 0.00097$ s) to study its effect on the mean slipstream boundary and total rotor thrust. The results of this are shown in Fig. 11, where it is seen that the slipstream boundary was insensitive to the value of time step, especially in the near wake. It can be concluded that for the range of time steps studied, the choice of time step does not affect VREM predictions.

The difference in normalized thrust coefficient compared to the baseline prediction is shown in Fig. 12 for different time steps. The margin of difference for this study was less than 0.2%, even when the time step was reduced by a factor of 10. This showed that the time step has a negligible effect on the convergence of the total rotor thrust.

4.1.7 Number of Rings. The total rotor thrust is shown in Fig. 7 as a function of vortex age for the baseline case of 1000 rings. It is seen that the thrust reached a steady state at a vortex age of 5400 deg, i.e., after 60 vortex rings were emitted.

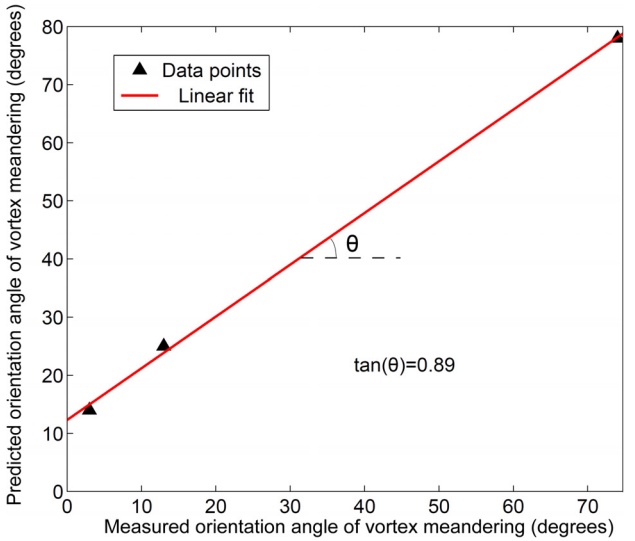

Fig. 14 Correlation between orientation of vortex aperiodicity predicted by VREM and measured by experiment, at 0 deg, 180 deg, and 270 deg vortex ages)

Therefore, it can be concluded that only 60 rings were required to obtain thrust convergence. The mean slipstream boundary is shown in Fig. 13 for different numbers of emitted rings. It can be seen that the shape of the slipstream boundary does not change significantly as the number of emitted rings exceeds 270.

4.1.8 Conclusions From the Sensitivity Study. The sensitivity of the mean slipstream boundary and rotor thrust to variations of the baseline parameters was found to be negligible. The rotor thrust converged rapidly after 60 rings were emitted whereas at least 270 vortex rings were required for slipstream boundary convergence. Therefore, a nominal value of 1000 rings was chosen for the VREM predictions. The time step (rpm dependence), initial tip vortex core radius, and viscosity parameter were chosen based on experimental conditions.

4.2 Vortex Aperiodicity Characterization. The VREM with the baseline values of parameters (Table 2) was used to calculate the positions of the vortex ring cores corresponding to various vortex ages. An ellipse was drawn around the 95% confidence region of tip vortex position for vortex ages of 90 deg, 180 deg, and 270 deg. The major axis of this elliptical region was aligned approximately perpendicular to the orientation of the slipstream boundary. The angle between the major axis of this elliptical region and the horizontal plane is plotted in Fig. 14 for both the VREM calculations and the experimental measurements. It can be seen that the VREM predictions of vortex aperiodicity orientation are in good agreement with the experiment. A linear correlation between the analysis and experiments was found to have a slope of 0.89. We conclude that the VREM can predict the orientation of vortex aperiodicity to within an error of ~10%, while the extent of the predicted aperiodicity was seen to be larger than the experimental measurements (Fig. 15). Therefore, the VREM is a computationally inexpensive way to calculate an anisotropic probability distribution function for vortex core positions that can then be used to correct measurements for vortex aperiodicity.

The VREM was run at different rotor collective pitch angles to obtain four values of blade loading, $C_t/\sigma = 0.0187, 0.042$, 0.0561, and 0.0704. The instantaneous tip vortex positions corresponding to 90 deg vortex age were determined for each case and 1000 such data points were plotted to observe the effect of blade loading on vortex aperiodicity. It is seen that the orientation of the aperiodicity is independent of C_t/σ. The extent of the aperiodicity increases with increased blade loading. The cases corresponding

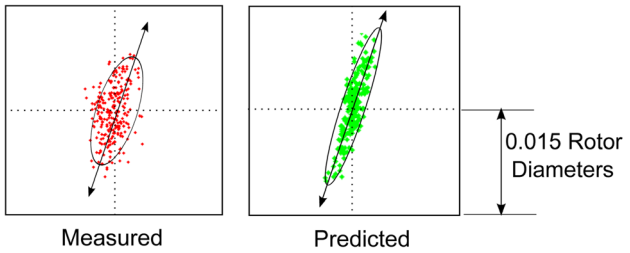

Fig. 15 Comparison between measured and predicted vortex core positions (250 samples) for vortex age of 90 deg. The dots represent instantaneous tip vortex positions at this vortex age. The arrow indicates the preferred direction of aperiodicity (major axis of the ellipse).

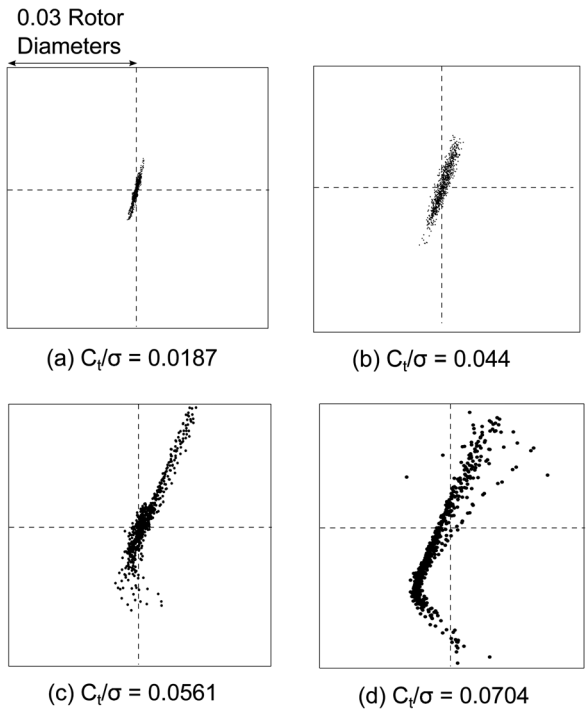

Fig. 16 Vortex aperiodicity predicted by the VREM at a vortex age of 90 deg for different values of blade loadings ($C_t/\sigma = 0.0187$, 0.042, 0.0561, and 0.0704). Each dot represents an instantaneous tip vortex position.

to lower blade loading (Figs. 16(*a*) and 16(*b*)) show a well-defined elliptical shape of vortex aperiodicity. With an increase in blade loading (Figs. 16(*c*) and 16(*d*)), the distribution of vortex aperiodicity appears to lose its elliptical form.

The increased aperiodicity (for cases corresponding to higher blade loadings) is expected to cause increased fluctuations in total rotor thrust. This trend can be seen in Fig. 17 where the total rotor thrust is plotted against vortex age for various values of blade loading. It is observed that for lower blade loadings ($C_t/\sigma = 0.0187, 0.042$), fluctuations in rotor thrust are not prominent. However, as the blade loading is increased, periodic fluctuations in the total rotor thrust are observed.

Note that the VREM relies on the approximation of the helical rotor wake as a series of toroidal vortex rings. At low blade loadings, i.e., when the rotor is producing low thrust, the induced velocity is low and the helix angle of the wake is small. In this case, the vortex ring approximation appears acceptable. However, at higher rotor thrust, the wake helix angle increases, and we can no longer expect the vortex ring structure to capture the dynamics of the wake. This is reflected in the increased thrust fluctuations at higher blade loadings, as shown in Fig. 17. We conclude that the

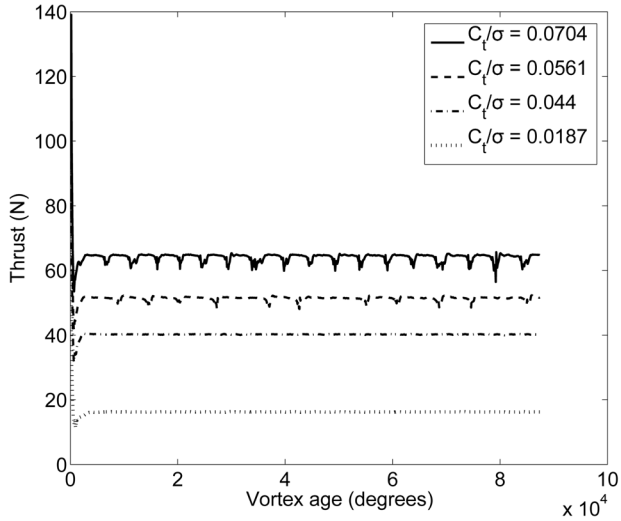

Fig. 17 Variation in rotor thrust as a function of vortex age for different values of blade loading

VREM is suitable for approximating the vortex aperiodicity for blade loadings $C_t/\sigma <\sim 0.05$.

5 Summary and Conclusions

In summary, a vortex ring emitter model (VREM) was developed to capture the anisotropic aperiodicity of tip vortices trailed from a hovering helicopter rotor. The model approximated the helical wake of the rotor as a series of toroidal vortex rings that were allowed to freely interact with each other. The effect of the vortex sheet emitted from the inboard sections of the rotor blade was ignored as it was not possible to represent the continuous vortex sheet using discrete vortex rings. Despite these simplifications, the VREM produced some very interesting results. The VREM predicted a well-defined slipstream boundary in the near wake, followed by a roll up in the far wake. The estimated rotor thrust converged to a steady state after around 60 rings were shed, with minor thrust fluctuations ($<0.5\%$). The shape of the spanwise loading was significantly different from that predicted by blade element momentum theory (BEMT) due to the simplification of a single concentrated tip vortex instead of a continuous vortex sheet trailing from the rotor blade. However, the thrust estimates by the VREM were found to be in very good agreement with BEMT (to within $\sim 5\%$) in steady state. Therefore, the VREM can be used for predicting global quantities, such as total rotor thrust, but is not accurate for calculating the induced velocity distribution at the rotor disk.

A detailed sensitivity study was conducted to validate the choice of the parameters used in the VREM. The sensitivity of the mean slipstream boundary shape and total rotor thrust to different values of initial tip vortex core radius, viscosity parameter, time step, and number of rings emitted was found to be negligible. Wake measurements were performed on a 1 m diameter, four-bladed rotor in hover using PIV. The extent of the predicted tip vortex anisotropy was qualitatively similar to measurements and the orientation of anisotropy was correlated to within 10%.

It is important to understand certain limitations of this approach. Most importantly, the VREM relies on approximating the helical wake as a series of toroidal vortex rings. Therefore, this approach cannot be expected to approximate the dynamics of the tip vortices at high disk loading when the helix angle becomes large and the three-dimensional nature of the helical vortex filaments becomes prominent. Also, the underlying assumption of one vortex ring being emitted from each blade per revolution limits the calculation of tip vortex positions to wake ages that are integral multiples of 360 deg $/N_b$, where N_b is the number of blades.

Finally, the VREM assumes that the vortex rings have a circular cross section while experiments have shown that this is often not the case. Within these limitations, the VREM has proved to be a computationally inexpensive method that can capture the dynamics of tip vortex anisotropy. This method can be used to calculate probability distribution functions for tip vortex core positions that can then be used in corrections of experimental measurements.

Acknowledgment

The work is supported by Army/Navy/NASA's Vertical Lift Research Center of Excellence (VLRCOE) Grant No. W911W6-11-2-0012 led by the University of Maryland with Dr. Mike Rutkowsky as Technical Monitor. The authors would also like to thank Mr. Mark Dreier, staff engineer, Bell Helicopter Textron Inc., for his guidance and support towards the development and testing of the analysis.

Nomenclature

A = area of the rotor disk, m^2
c = chord length of a rotor blade, m
C_t = rotor thrust coefficient, $T/(\rho A(\Omega R)^2)$
N_b = number of rotor blades
R_ζ = radius of vortex ring at a vortex age of ζ, m
r_i^n = radial position of the ith vortex ring at the nth time step, m
r_i^* = radial position of the ith vortex ring at the intermediate time step, m
r_{core} = core radius of a vortex ring, m
$r_{\text{core},\zeta}$ = core radius of a vortex ring at a vortex age of ζ, m
$r_{\text{core},\zeta,\text{s}}$ = core radius of a vortex ring at a vortex age of ζ due to filament strain, m
$r_{\text{core},\zeta,\nu}$ = core radius of a vortex ring at a vortex age of ζ due to viscous diffusion, m
Vi_x = radial velocity of a vortex ring, m/s
Vi_z = axial velocity of a vortex ring, m/s
V_{tip} = tip speed of rotor blade, m/s
z_i^n = axial position of the ith vortex ring at the nth time step, m
z_i^* = axial position of the ith vortex ring at the intermediate time step, m
Δt = blade passage time (time step), s
ρ = density of air, kg/m^3
σ = rotor solidity, $N_b c/\pi R$
θ_0 = collective angle at the blade root, rad
Ω = rotational speed of the rotor, rad/s
ζ = age of a vortex ring (vortex age), rad

References

[1] Landgrebe, A. J., 1972, "The Wake Geometry of a Hovering Helicopter Rotor and Its Influence on Rotor Performance," J. Am. Helicopter Soc., **17**(4), pp. 3–15.
[2] Devenport, W. J., Rife, M. C., Liapis, S. I., and Follin, G. J., 1996, "The Structure and Development of a Wing-Tip Vortex," J. Fluid Mech., **312**, pp. 67–106.
[3] Leishman, J. G., 1998, "Measurements of the Aperiodic Wake of a Hovering Rotor," Experiments Fluids, **25**(4), pp. 352–361.
[4] Bhagwat, M. J. and Ramasamy, M., 2012, "Effect of tip vortex aperiodicity on measurement uncertainty," Experiments Fluids, **53**, pp. 1191–1202.
[5] Richard, H., Bosbach, J., Henning, A., Raffel, M., and van der Wall, B., 2006, "2c and 3c PIV Measurements on a Rotor in Hover Condition," 13th International Symposium on Applications of Laser Techniques to Fluid Mechanics, Lisbon, Portugal, June 26–29.
[6] van der Wall, B. G., and Richard, H., 2006, "Analysis Methodology for 3c-PIV Data of Rotary Wing Vortices," Experiments Fluids, **40**(5), pp. 798–812.
[7] Kindler, K., Mulleners, K., Richard, H., van der Wall, B. G., and Raffel, M., 2011, "Aperiodicity in the Near Field of Full-Scale Rotor Blade Tip Vortices," Experiments Fluids, **50**(6), pp. 1601–1610.
[8] Mula, S., Stephenson, J., Tinney, C., and Sirohi, J., 2011, "Vortex Jitter in Hover," AHS Southwest Region Technical Specialists's Meeting, Fort Worth, TX, February 23–25.
[9] Bagai, A., and Leishman, J. G., 1995, "Rotor Free-Wake Modeling Using a Pseudo-Implicit Technique-Including Comparisons With Experimental Data," J. Am. Helicopter Soc., **40**(3), pp. 29–41.
[10] Bhagwat, M. J., and Leishman, J. G., 2001, "Stability, Consistency and Convergence of Time-Marching Free-Vortex Rotor Wake Algorithms," J. Am. Helicopter Soc., **46**(1), pp. 59–71.
[11] Bhagwat, M. J., and Leishman, J. G., 2003, "Rotor Aerodynamics During Maneuvering Flight Using a Time-Accurate Free-Vortex Wake," J. Am. Helicopter Soc., **48**(3), pp. 143–158.
[12] Ramasamy, M., and Leishman, J. G., 2003, "The Interdependence of Straining and Viscous Diffusion Effects on Vorticity in Rotor Flow Fields," American Helicopter Society 59th Annual National Forum, Phoenix, AZ, May 6–8.
[13] Bhagwat, M. J., and Leishman, J. G., 2002, "Generalized Viscous Vortex Core Models for Application to Free-Vortex Wake and Aeroacoustic Calculations," Proceedings of the 58th Annual Forum of the American Helicopter Society International, Montréal, Canada.
[14] Young, L. A., 2003, "Vortex Core Size in the Rotor Near-Wake," NASA Technical Report TM-2003-212275.
[15] Brand, A., Dreier, M., Kisor, R., and Wood, T., 2011, "The Nature of the Vortex Ring State," J. Am. Helicopter Soc., **56**(2), p. 22001.
[16] McCroskey, W. J., 1995, "Vortex Wakes of Rotorcraft," 33th Aerospace Sciences Meeting and Exhibit, Reno, NV, January 9–12, Paper No. AIAA 95-0530.
[17] Mula, S., Stephenson, J., Tinney, C., and Sirohi, J., 2012, "Dynamical and Evolutionary Characteristics of the Tip Vortex From a Four Bladed Rotor in Hover," American Helicopter Society 68th Annual Forum, Fort Worth, TX, May 1–3.
[18] Squire, H. B., 1965, "The Growth of a Vortex in Turbulent Flow," Aeronaut. Qtr., **16**, pp. 302–306.
[19] Bhagwat, M. J., and Leishman, J. G., 2000, "Stability Analysis of Helicopter Rotor Wakes in Axial Flight," J. Am. Helicopter Soc., **45**(3), pp. 165–178.